Original article

MOLECULAR METABOLISM

Acyl CoA synthetase 5 (ACSL5) ablation in mice increases energy expenditure and insulin sensitivity and delays fat absorption

Thomas A. Bowman [1], Kayleigh R. O'Keeffe [1], Theresa D'Aquila [3], Qing Wu Yan [1], John D. Griffin [1], Elizabeth A. Killion [1], Deanna M. Salter [1], Douglas G. Mashek [2], Kimberly K. Buhman [3], Andrew S. Greenberg [1,*]

ABSTRACT

Objective: The family of acyl-CoA synthetase enzymes (ACSL) activates fatty acids within cells to generate long chain fatty acyl CoA (FACoA). The differing metabolic fates of FACoAs such as incorporation into neutral lipids, phospholipids, and oxidation pathways are differentially regulated by the ACSL isoforms. *In vitro* studies have suggested a role for ACSL5 in triglyceride synthesis; however, we have limited understanding of the *in vivo* actions of this ACSL isoform.

Methods: To elucidate the *in vivo* actions of ACSL5 we generated a line of mice in which ACSL5 expression was ablated in all tissues ($ACSL5^{-/-}$).

Results: Ablation of ACSL5 reduced ACSL activity by ~80% in jejunal mucosa, ~50% in liver, and ~37% in brown adipose tissue lysates. Body composition studies revealed that $ACSL5^{-/-}$, as compared to control $ACSL5^{loxP/loxP}$, mice had significantly reduced fat mass and adipose fat pad weights. Indirect calorimetry studies demonstrated that $ACSL5^{-/-}$ had increased metabolic rates, and in the dark phase, increased respiratory quotient. In $ACSL5^{-/-}$ mice, fasting glucose and serum triglyceride were reduced; and insulin sensitivity was improved during an insulin tolerance test. Both hepatic mRNA (~16-fold) and serum levels of fibroblast growth factor 21 (FGF21) (~13-fold) were increased in $ACSL5^{-/-}$ as compared to $ACSL5^{loxP/loxP}$. Consistent with increased FGF21 serum levels, uncoupling protein-1 gene (*Ucp1*) and PPAR-gamma coactivator 1-alpha gene (*Pgc1α*) transcript levels were increased in gonadal adipose tissue. To further evaluate ACSL5 function in intestine, mice were gavaged with an olive oil bolus; and the rate of triglyceride appearance in serum was found to be delayed in $ACSL5^{-/-}$ mice as compared to control mice.

Conclusions: In summary, $ACSL5^{-/-}$ mice have increased hepatic and serum FGF21 levels, reduced adiposity, improved insulin sensitivity, increased energy expenditure and delayed triglyceride absorption. These studies suggest that ACSL5 is an important regulator of whole-body energy metabolism and ablation of ACSL5 may antagonize the development of obesity and insulin resistance.

Keywords Dietary fat absorption; Acyl-CoA; ACSL; Intestine; Liver; FGF21

1. INTRODUCTION

Alterations in fatty acid trafficking and metabolism have been implicated as critical factors in the development of obesity and its associated complications such as non-alcoholic fatty liver disease (NAFLD), and type2 diabetes (T2DM) [1–4]. Central to our understanding of fatty acid trafficking are proteins that determine the metabolic fate of fatty acids. The first step in intracellular metabolism of fatty acids is the addition of a CoA group catalyzed by the actions of long-chain acyl-CoA synthetases (ACSL) [5,6]. Five related ACSL isoforms have been delineated in rats, mice and humans [5,7]. It has been hypothesized that the different ACSL isoforms may direct fatty acids to different metabolic fates depending upon the protein's subcellular localization and tissue specific expression [6].

At the present time, we have limited understanding about the relative contributions of acyl CoA synthetase 5 (ACSL5) to *in vivo* lipid

[1]Jean Mayer USDA Human Nutrition Research Center on Aging, Tufts University, Boston, MA, USA [2]Department of Food Science and Nutrition, University of Minnesota, St. Paul, MN, USA [3]Department of Nutrition Science, Purdue University, West Lafayette, IN, USA

*Corresponding author.

E-mails: thomas.bowman@tufts.edu (T.A. Bowman), kokeeffe@live.unc.edu (K.R. O'Keeffe), tdaquila@gmail.com (T. D'Aquila), qing-wu.yan@tufts.edu (Q.W. Yan), john.griffin@tufts.edu (J.D. Griffin), elizabeth.killion@tufts.edu (E.A. Killion), deanna.salter@tufts.edu (D.M. Salter), dmashek@umn.edu (D.G. Mashek), kbuhman@purdue.edu (K.K. Buhman), andrew.greenberg@tufts.edu (A.S. Greenberg).

Abbreviations: ACSL, long-chain acyl-CoA synthetase; ACSL5−/−, mice with global ablation of ACSL5; FGF21, fibroblast growth factor 21; UCP1, uncoupling protein-1; PPAR, peroxisome proliferator activated receptor; PGC1α, PPAR-gamma coactivator 1α; NAFLD, non-alcoholic fatty liver disease; T2DM, type2 diabetes; SREBP1c, steroid response element binding protein-1c; VLDL, very low density lipoprotein; ES, embryonic stem; ITT, insulin tolerance test; SDS, sodium dodecyl sulfate; AUC, area under the curve; RER, respiratory exchange ratio

Received October 21, 2015 • Revision received December 22, 2015 • Accepted January 3, 2016 • Available online 11 January 2016

http://dx.doi.org/10.1016/j.molmet.2016.01.001

metabolism. ACSL5 has been reported to be highly expressed in liver, small intestine, white preadipocytes, and brown adipose tissue [7,8]. Hormonal regulation of hepatic ACSL5 expression was suggested by the observation that both fasting and streptozocin-induced diabetes reduced ACSL5 expression, while carbohydrate feeding increased the protein's expression [7–9]. These prior observations indicated that insulin and its downstream mediators such as the nuclear transcription factor, SREBP-1C, regulate ACSL5 expression [10,11]. A role for SREBP1c in regulating ACSL5 expression was demonstrated when adenoviral mediated overexpression of SREBP1c in rats with streptozocin-induced diabetes rescued hepatic ACSL5 expression [9,10].

Overexpression of ACSL5 in rat hepatoma McCardle-RH777 cells increased both fatty acid uptake and conversion of fatty acids to triacylglycerol [7]. Additionally, siRNA mediated knockdown of ACSL5 in isolated rat hepatocytes reduced triglyceride accumulation and VLDL secretion while increasing fat oxidation [12]. Furthermore, studies of rodents have demonstrated that ACSL5 is most highly expressed within jejunal enterocytes [8], which alludes to the possibility that ACSL5 may be involved in fat absorption during the reesterification of dietary fatty acids into triglyceride. In jejunal enterocytes, triglyceride is packaged and secreted as chylomicrons that ultimately circulate in the blood. Importantly, ACSL5 was found to be present on cytoplasmic lipid droplets in jejunal enterocytes [13]. However, at the present time we have little understanding of ACSL5's role in intestinal lipid metabolism.

As a first step to elucidating the *in vivo* role of ACSL5 in tissue specific and systemic metabolism, our laboratory has generated mice in which ACSL5 expression is ablated in all tissues ($ACSL5^{-/-}$). Investigations of these mice demonstrate that loss of ACSL5 expression significantly reduced total ACSL activity in liver, brown adipose tissue, and most robustly within jejunum. Intriguingly, ablation of ACSL5 resulted in increased hepatic mRNA and serum FGF21 levels in mice consuming a chow diet. Consistent with increased FGF21 expression, $ACSL5^{-/-}$ mice have increased metabolic rate, reduced fat mass and serum TG, improved insulin sensitivity, and increased expression of UCP1 in white adipose tissue depots. Interestingly, triglyceride absorption studies demonstrated a role for ACSL5 in dietary fat absorption.

2. MATERIALS AND METHODS

2.1. Generation of ACSL5 deficient mice ($ACSL5^{-/-}$)

We collaborated with Genoway (Lyon, France) to generate a line of conditional ACSL5 knockout mice. The ACSL5 gene was isolated from a C57BL6/J library and loxP sequences inserted in introns flanking exons 16 and 17 (exons nomenclature based on NM_027976.2 sequence). The ACSL5 gene construct was introduced in C57BL6/J embryonic stem (ES) cells; ES cells were selected for homologous recombination, injected into mice, and progeny were mated to generate line of mice in which the ACSL5 gene was floxed ($ACSL5^{loxP/loxP}$) (See Figure 1). Selection of recombined construct in C57BL6/J ES

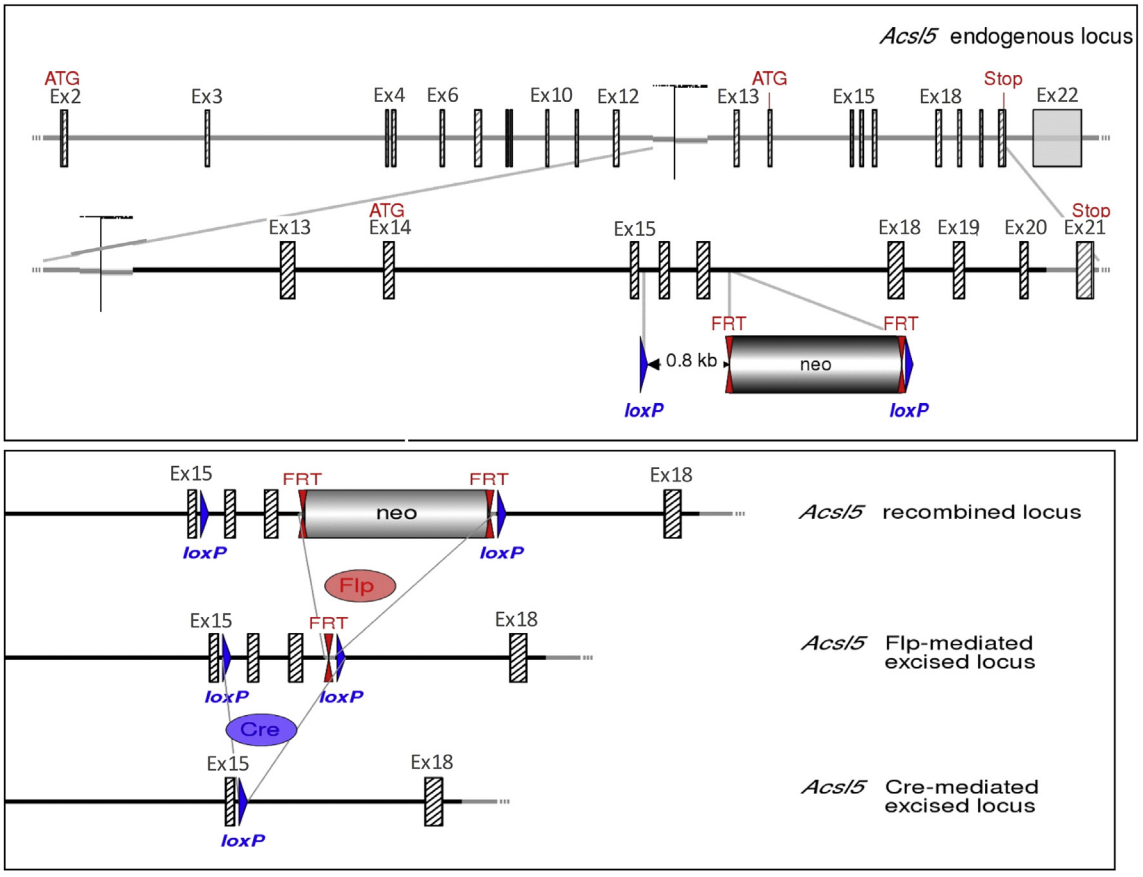

Figure 1: Schematic representation of *Acsl5* targeting strategy, resulting in deletion of exons 16–17. Diagram is not depicted to scale. Hatched rectangles represent Acsl5 coding sequences, gray rectangles indicate non-coding exon portions, and solid lines represent chromosome sequences. In upper panel, the initiation (ATG) and Stop (Stop) codons are indicated. FRT sites are represented by double red triangles and loxP sites by blue triangles. The size of the flanked Acsl5 sequence to be deleted is shown. The strategy results in the deletion of 206 bp of coding sequences encoding for part of the AMP binding domain. The splicing of exon 15 to exon 18 will lead to a frame shift resulting in a premature stop codon in exon 20. In lower panel, the scheme of Cre recombinase- or Flp recombinase-mediated excision at the recombined Acsl5 locus.

cells was aided by inclusion of a FRT flanked neomycin cassette. The neomycin cassette and flanking FRT sequences were removed by mating chimeric mice to mice expressing flip recombinase. Mice were mated to a line of transgenic mice, on a congenic C57BL6J background, expressing Cre in all tissues to ultimately generate a line of ACSL5 deficient mice (*ACSL5*$^{-/-}$). The Cre-mediated excision of exons 16 and 17 results in transcription of a sequence with a frame shift resulting in a premature stop codon in exon 18.

To generate ACSL5 deficient mice, *ACSL5*$^{loxP/loxP}$ mice were mated to a line of wild type (ACSL5$^{+/+}$) transgenic mice (on a congenic C57BL6J background), which expressed a CMV Cre construct germline (Genoway). This transgenic mouse, generated at Genoway, was generated by injecting a CMV-Cre construct into C57BL/6 embryos which gave rise to a proprietary transgenic line which ubiquitously expressed Cre recombinase. From the progeny of these matings, mice were selected that were deficient in ACSL5 (ACSL5$^{-/-}$) but did not express Cre; and these mice were used in subsequent matings to transmit the ablated ACSL5 allele to progeny because the transgene construct for Cre was expressed germline. The absence of ACSL5 in ACSL5$^{-/-}$ mouse tissues was confirmed by RT-PCR and western blot. Homozygous mouse lines of *ACSL5*$^{-/-}$ and *ACSL5*$^{loxP/loxP}$ were generated, and ACSL5$^{-/-}$ mice were mated to *ACSL5*$^{loxP/loxP}$ mice to generate male and female mice, which were heterozygous for the ACSL5 null allele and floxed allele (*ACSL5*$^{loxP/-}$). For all experiments male and female *ACSL5*$^{loxP/-}$ mice were mated to each other and from the progeny littermate male *ACSL5*$^{loxP/loxP}$ and ACSL5$^{-/-}$ mice were identified and used for experiments.

2.2. Animal care

Experiments were conducted in a viral pathogen-free facility at the Jean Mayer-U.S. Department of Agriculture Human Nutrition Research Center on Aging at Tufts University and at Purdue University in accordance with Institutional Animal Care and Use Committees guidelines. Experimental male ACSL5 knockout and littermate floxed control mice were generated from heterozygous matings as described above and in the results section. Genotyping of weaned mice was confirmed by RT-PCR at sacrifice. All mice were provided *ad libitum* a purified standard diet from birth (2016S, Teklad). In these male mice, body weights and magnetic resonance (EchoMRI-700) fat and lean mass body composition data were monitored and repeated in two generations of male mice. At 4 months of age an insulin tolerance test (ITT) was performed (and repeated from two different generations of mice) with 0.75 units of insulin per kilogram body weight injected intraperitoneally after a 6 h morning fast, and blood obtained by tail vein at six time points for glucose measurements. Indirect calorimetry (TSE Systems) metabolic cages were utilized to evaluate oxygen consumption, carbon dioxide expenditure, and activity by infrared counts of all animal movement. Measurements were made in metabolic cages (4 mice per group average of 2 days after initial 48 h acclimation period, bedding was transferred from cages mice had using before). These studies were repeated in two separate generations of male mice. The resulting respiratory exchange ratios and energy expenditure values were calculated from these measurements. Mice were sacrificed by carbon dioxide narcosis at ~6 months of age and blood collected by cardiac puncture, tissues were dissected, weighed, and snap frozen for analysis, or were fixed, embedded in paraffin, and sectioned for histological analysis. For studies investigating the intestine, during sacrifice, the small intestine was isolated, divided into three equal-length sections on ice at the time of sacrifice in order to obtain cross-sections for histology and mucosal scrapings were obtained for RT-PCR and western blot analyses. The first proximal third of the small intestine was designated as duodenum. The second middle third of the small intestine was designated as jejunum. And the last distal third of the small intestine was designated as ileum.

2.3. Triglyceride secretion studies

In triglyceride secretion assays in response to dietary fat, male mice were fasted for 4 h, starting at the beginning of the light cycle [14–16]. Mice were then injected with tyloxapol (500 mg/kg) IP. Thirty minutes after tyloxapol injection, blood was collected via submandibular bleed for analysis of plasma triglyceride concentrations (Time 0). Mice were then immediately gavaged with 200 μl of olive oil and blood collected via submandibular bleed at 2 and 4 h post gavage for plasma triglyceride analysis. Plasma triglyceride concentrations were determined by Wako L-Type TG M kit (Wako Chemicals USA).

2.4. RT-PCR

Adipose tissue, brain, intestinal mucosal scrapings and spleen RNA was extracted using Qiagen Lipid Mini kits and liver RNA was isolated using Qiagen Mini kits according to manufacturer's instructions. RNA was quantified and checked for purity using the Nanodrop spectrophotometer (Nanodrop 1000, Wilmington, DE). cDNA was generated from 1 μg of RNA, and real-time quantitative PCR was performed using SYBR Green (Applied Biosystems 7300, Carlsbad, CA). Fold-changes were calculated as $2^{-\Delta\Delta CT}$, with cyclophilin B used as the endogenous control. Primer sequences are listed in Table S1.

2.5. Western blot

Protein lysates of tissues were centrifuged at 100,000 g for sixty minutes to remove neutral lipid. 25 μg of the homogenized protein lysates were solubilized and denatured by boiling five minutes in 1× sodium dodecyl sulfate (SDS) solution with 2-mercaptoethanol, which were resolved by loading into wells of 7.5% polyacrylamide gel (Mini Protean TGX, BioRad) and run with 1× tris-glycine-SDS buffer, transferred to nitrocellulose membrane, and blocked with 5% bovine serum albumin in tris-buffered saline with 0.2% tween. For demonstration of the presence or lack of ACSL5 protein content in Figure 2B, we generated and utilized an affinity purified rabbit polyclonal antibody directed against the peptide CDTPQKATMLVENVEKG located in the ACSL5 amino terminus (5N-1) that was diluted 1:1000, and also reprobed for normalization with 1:5000 dilution of GAPDH antibody raised in rabbit (14C10, Cell Signaling, see lower panel). The secondary antibody, donkey anti-rabbit horseradish peroxidase (GE Healthcare UK), was diluted 1:10,000 prior to 1 h membrane incubation and detected by chemiluminescence images captured with a sensitive camera (Fluorchem Q, Alpha Innotech).

2.6. Acyl CoA synthetase enzyme activity

Acyl CoA synthetase enzyme activity was performed as in [17,18]. Protein lysates of tissues were centrifuged at 100,000 g for sixty minutes to separate the membrane pellet from the cytoplasm. The cytoplasm was discarded, and the membrane pellet, which included the mitochondrial and microsomal fractions, was recovered and used to measure acyl CoA synthetase activity. We determined ACSL activity with 2–6 μg of protein, which was found to be in the linear range for enzyme activity for all three tissues. We utilized 100 μM [1-^{14}C] palmitic acid (Perkin–Elmer) incubated at room temperature for 10 min, 10 mM ATP, 250 mM CoA, 5 mM DTT, and 8 mM $MgCl_2$ in 175 mM Tris, pH 7.4; and stopped the reaction with Dole's solution. We performed two sequential washes of the organic phase from heptane-water extractions. Aqueous phase radioactivity of the resulting Acyl CoAs was measured by scintillation counter.

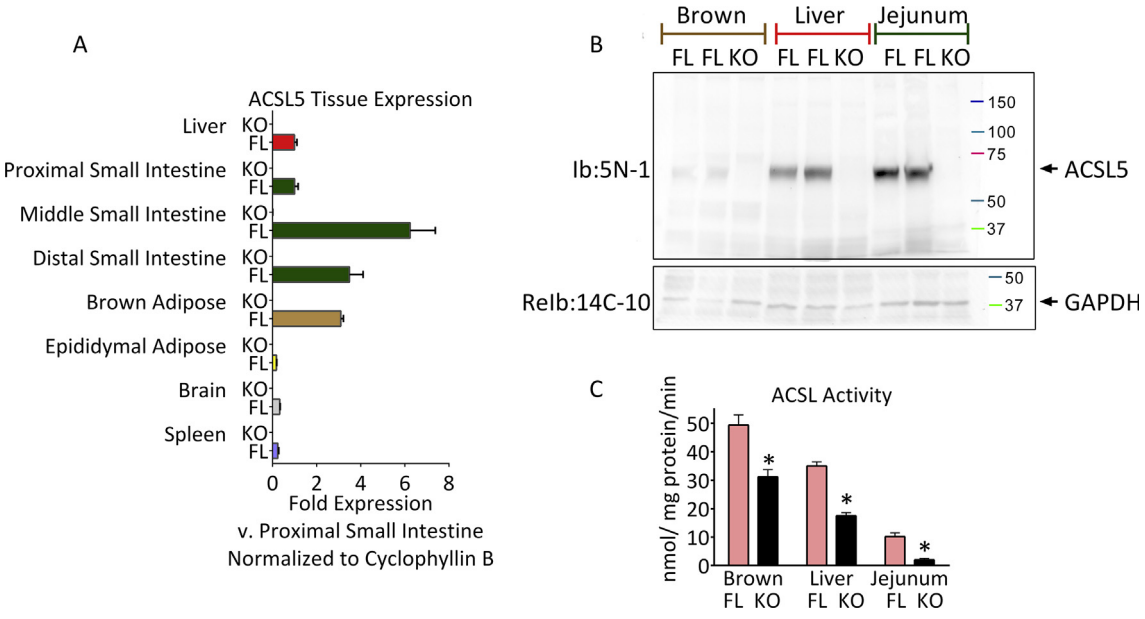

Figure 2: Tissue survey of mRNA and protein expression of ACSL5 and demonstration of lack of ACSL5 protein content and decreased ACSL activity in *ACSL5*$^{-/-}$ mice. Tissues mRNA and protein were analyzed (see Methods) of 6 month old *ACSL5*$^{-/-}$ and their littermate male *ACSL5*$^{loxP/loxP}$ floxed control mice as generated in Figure 1. In panel A, mean mRNA fold expression of Acsl5 +/− standard error of the mean (SEM) of the indicated tissues of 4–9 mice in each group were determined by semi-quantitative real-time RT-PCR, normalized to *Cyclophyllin B*, and normalized again to the mean result of the proximal small intestine. Equal protein amounts (in panel B) of protein lysates were resolved by western blot with 5N-1 antibody (see Methods) for ACSL5, producing a single band at approximately 65 kDa. The membrane was reprobed with antibody for GAPDH for loading control. In C, ACSL activity presented as means ± SEM of 3–4 mice was determined by incubation of lysates with 100 μM [1-^{14}C] palmitic acid (see Methods), *$p < 0.05$ ACSL comparing *ACSL5*$^{-/-}$ (KO) and *ACSL5*$^{loxP/loxP}$ (FL).

2.7. Blood and plasma biochemistry

Whole blood glucose measurements were made by glucometer (One Touch Ultra Blue, LifeScan, Inc). Blood plasma was obtained by cardiac puncture. The plasma supernatant of low speed centrifugation was analyzed by ELISA for mouse insulin (Ultra-sensitive mouse insulin, Crystal Chem, Inc), and by enzymatic endpoint for β-hydroxybutyrate (β-hydroxybutyrate dehydrogenase, Stanbio), and enzymatic colorimetric endpoint assay (Beckman Coulter AU400) for triglyceride (glycerol phosphate oxidase, Beckman Coulter OSR6133) and cholesterol (Aminoantipyrine/Phenol/Peroxidase, Beckman Coulter OSR6116) content. Serum and liver free fatty acids were determined using the Wako NEFA HR(2) kit from serum and liver lipid from Folch 2:1 chloroform:methanol organic layer extract dried and resuspended in 1% Triton. Liver free fatty acids were normalized to protein content of aqueous layer by bicinchoninic acid assay (Thermo Scientific Pierce).

2.8. Liver triglyceride analysis

Liver triglyceride was determined by modified Folch procedure [19–21]. Snap frozen wet liver was homogenized in 2:1 chloroform:methanol with overnight incubation and subsequent extraction with magnesium chloride; the organic layer was evaporated under nitrogen at 37 °C to complete dryness and saponified by incubating with ethanolic potassium hydroxide solution at 60 °C for one hour and adding magnesium sulfate. The resultant supernatant was evaluated for liberated glycerol (Sigma) [19–21].

2.9. Statistical analysis

The results are expressed as means ± standard error of the mean (SEM). All comparisons of control (*ACSL5*$^{loxP/loxP}$) vs. knockout (*ACSL5*$^{-/-}$) mice were made using an unpaired two-tailed Student's *t*-test and graphed by GraphPad Prism 6.04. For analyses of control vs. knockout mice, p values <0.05 were designated as significant and labeled in table and figures with an asterisk (*). Statistical analyses were not performed on comparisons between tissues on tissue surveys beyond noting the significant absence of ACSL5 mRNA and protein in all *ACSL5*$^{-/-}$ tissues, as there were insufficient data and only a qualitative inference was made.

3. RESULTS

3.1. Generation of *ACSL5*$^{-/-}$ mice and characterization of ACSL expression and activity

To determine the *in vivo* role of ACSL5 in tissue and systemic metabolism, we generated a line of mice in which we could ablate ACSL5 expression. The ACSL5 gene was targeted with insertion of loxP sites in the introns flanking exons 16 and 17; the construct was introduced into C57BL/6J embryonic stem cells, screened for homologous recombination, and then used to generate mice homozygous for the targeted gene (*ACSL5*$^{loxP/loxP}$) (See Figure 1). Complete details of the generation of these mice including targeting vector are described in the experimental sections. To generate ACSL5 deficient mice, *ACSL5*$^{loxP/loxP}$ mice were mated to a line of transgenic mice that expressed Cre germline in all tissues (CMV-Cre), producing F2 and subsequent progeny (*ACSL5*$^{-/-}$) with permanent ablation of ACSL5 in the absence of the CMV-Cre transgene, which was bred out of the colony. For all experiments male and female mice heterozygous for the ACSL5-deficient allele and the floxed allele (*ACSL5*$^{loxP/-}$) were mated to each other and from the progeny, littermate male *ACSL5*$^{loxP/loxP}$ and ACSL5$^{-/-}$ mice were identified and used for experiments.

To determine the pattern of ACSL5 tissue expression in *ACSL5*$^{loxP/loxP}$ and *ACSL5*$^{-/-}$ male mice consuming a chow diet [7,8] we analyzed

Table 1 — ACSL gene expression in *ACSL5*$^{loxP/loxP}$ and *ACSL5*$^{-/-}$ mice. Mean mRNA fold expression (see Methods) ± SEM of mucosal scrapings of the small intestine, liver and interscapular brown adipose tissue of 5—7 mice after a 3 h morning fast were determined by semi-quantitative real-time RT-PCR, normalized to Cyclophyllin B, and normalized again to the mean result of each gene in floxed control *ASCL5*$^{loxP/loxP}$ (FL) mice samples; * ($p < 0.05$) indicates significant difference between *ACSL5*$^{loxP/loxP}$ and *ACSL5*$^{-/-}$ for each gene comparison.

		Acsl1	*Acsl3*	*Acsl4*	*Acsl5*
Jejunum	*ACSL5*$^{loxP/loxP}$	1.00 ± 0.24	1.00 ± 0.22	1.00 ± 0.24	1.00 ± 0.18
	ACSL5$^{-/-}$	1.02 ± 0.27	1.38 ± 0.43	0.63 ± 0.20	<0.01*
Liver	*ACSL5*$^{loxP/loxP}$	1.00 ± 0.09	1.00 ± 0.11	1.00 ± 0.11	1.00 ± 0.12
	ACSL5$^{-/-}$	0.50 ± 0.05*	1.43 ± 0.19	1.66 ± 0.22*	<0.01*
Brown adipose	*ACSL5*$^{loxP/loxP}$	1.00 ± 0.10	1.00 ± 0.17	1.00 ± 0.17	1.00 ± 0.04
	ACSL5$^{-/-}$	0.75 ± 0.08	0.58 ± 0.06*	0.88 ± 0.14	<0.01*

mRNA levels by RT-PCR. We found highest expression of *Acsl5* mRNA in brown adipose tissue, liver, and in jejunal mucosa while mRNA levels of *Acsl5* were difficult to detect in gonadal white adipose tissue, spleen and brain (Figure 2A). ACSL5 protein levels were determined by Western blot and found in *ACSL5*$^{-/-}$ to be virtually absent in liver, brown adipose tissue and jejunal mucosa lysates (Figure 2B). Consistent with a previous report by Oikawa et al. which found highest levels of *Acsl5* mRNA in rat jejunum [8], we observed in control *ACSL5*$^{loxP/loxP}$ mice highest levels of *Acsl5* mRNA and protein in mouse jejunum. We next determined whether ACSL5-deficiency was associated with alterations in mRNA expression of other ACSL isoforms. In the jejunum of ACSL5 deficient mice we observed no significant changes in *Acsl1*, *3*, or *Acsl4* mRNA expression (see Table 1). While in brown adipose tissue of *ACSL5*$^{-/-}$ mice, we found 42% less *Acsl3* mRNA than in control mice; however similar levels of *Acsl1* and *Acsl4* mRNA levels compared to control mice. Finally, in liver we observed increased mRNA levels (~66%) for *Acsl4* and a 50% reduction in *Acsl1* mRNA levels compared to control mice. We next investigated the consequences of ACSL5 ablation on total ACSL activity in tissues where ACSL5 is highly expressed. Ablation of ACSL5 expression potently reduced ACSL activity in jejunum mucosal lysates by ~80% (see Figure 2C) consistent with ACSL5 being the predominant ACSL in jejunum [8]. While in liver and brown adipose lysates of *ACSL5*$^{-/-}$ mice, total ACSL activity was reduced by ~50% and ~37% respectively (see Figure 2C). In summary, these data confirm the

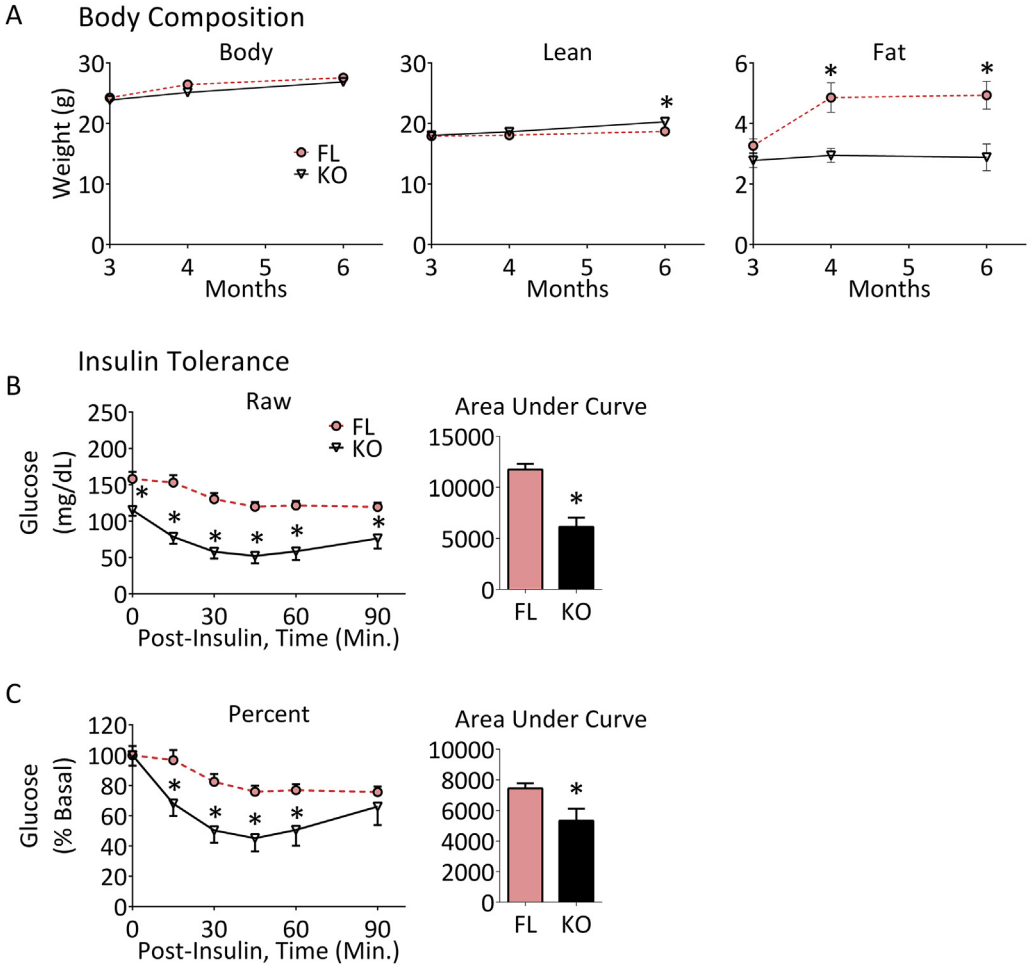

Figure 3: Reduced fat mass over time and improved insulin tolerance of *ACSL5*$^{-/-}$ mice. *ACSL5*$^{-/-}$ (KO) male mice and their littermate male *ACSL5*$^{loxP/loxP}$ floxed control (FL) mice were fed a standard purified diet (see Methods). Shown (A, Body Composition) are body weights, lean and fat mass measured using magnetic resonance at 3, 4 and 6 months of age. Insulin tolerance showing mean ± SEM of raw (B) and percent (C) glucose response to 0.75 mg/kg of insulin administered intraperitoneally of four-month-old male mice were determined (see Methods, n = 8—10 mice per group). Each time point and for Insulin Tolerance Area Under Curve were compared by student's t-test between ACSL5$^{-/-}$ (KO) and their littermate male *ACSL5*$^{loxP/loxP}$ floxed control (FL) mice, significance is indicated by *($p < 0.05$).

generation of an ACSL5 deficient mouse and that ACSL5 expression contributes significantly to total ACSL activity in liver, brown adipose tissue, and jejunum.

3.2. *ACSL5*$^{-/-}$ mice have reduced fat mass and improved insulin-glucose homeostasis

We determined both the body weights and body composition of both *ACSL5*$^{-/-}$ and *ACSL5*$^{loxP/loxP}$ mice over time (Figure 3). The body weights of male *ACSL5*$^{loxP/loxP}$ and *ACSL5*$^{-/-}$ mice did not differ as they aged, however MRI analysis of body composition demonstrated that starting at 4 months of age *ACSL5*$^{-/-}$ mice had significantly less total fat mass (~65% less at 4 months of age, ~71% less at 6 months) as compared to *ACSL5*$^{loxP/loxP}$ littermates (Figure 3, Table 2). In contrast to this lower fat mass by 6 months of age, *ACSL5*$^{-/-}$ were found to have a slight but significantly greater lean mass than *ACSL5*$^{loxP/loxP}$ mice.

At sacrifice, consistent with the MRI results, weights of both subcutaneous and gonadal fat tissues (Table 2) were significantly less in male *ACSL5*$^{-/-}$ mice. The liver weights of *ACSL5*$^{-/-}$ mice were also lower as compared to *ACSL5*$^{loxP/loxP}$ mice, but liver triglyceride content did not differ between the two lines of mice (Table 2). Serum levels of triglyceride, but not serum β-hydroxybutyrate or free fatty acid levels were significantly lower in *ACSL5*$^{-/-}$ mice compared to control mice. While fasting insulin levels did not differ between the two lines of mice, fasting blood glucose was 37% lower in *ACSL5*$^{-/-}$ mice as compared to littermate *ACSL5*$^{loxP/loxP}$ mice (Table 2). To better quantitate insulin sensitivity, insulin tolerance tests (ITT) were performed and demonstrated improved insulin sensitivity in ACSL5 deficient mice (Figure 3B). Since fasting blood glucose was lower in *ACSL5*$^{-/-}$ mice, we also analyzed the ITT data by normalizing the zero time glucose in both groups to 100%; and confirmed that with this approach as well that the area under the curve (AUC) was significantly lower (Figure 3C). Thus, *ACSL5*$^{-/-}$ mice have both lower fasting blood glucose and improved insulin tolerance as compared to mice expressing ACSL5.

Table 2 — Biochemistry and body composition in *ACSL5*$^{loxP/loxP}$ and *ACSL5*$^{-/-}$ mice. Mice fed a standard purified diet (see Methods) were analyzed for body weight, lean and fat mass measured using magnetic resonance at 6 months of age. The mice were sacrificed after a three hour morning fast and their liver and fat depots were resected (weights shown). Whole blood glucose measurements (by glucometer) are shown and blood plasma obtained by cardiac puncture was analyzed for insulin, â-hydroxybutyrate, free fatty acids and triglyceride (see Methods). Liver free fatty acids and triglyceride were determined as described in methods. Data are presented as means ± SEM of 5—7 mice, *p < 0.05 for each measurement comparison between *ASCL5*$^{loxP/loxP}$ and *ACSL5*$^{-/-}$.

	ACSL5$^{loxP/loxP}$	*ACSL5*$^{-/-}$
Body weight (g)	28.54 ± 0.72	27.12 ± 0.94
Lean mass (g)	18.70 ± 0.17	20.27 ± 0.20*
Fat mass (g)	4.93 ± 0.46	2.88 ± 0.44*
Liver (g)	1.19 ± 0.04	0.74 ± 0.04*
Subcutaneous fat (g)	0.44 ± 0.04	0.29 ± 0.03*
Gonadal fat (g)	0.81 ± 0.07	0.37 ± 0.04*
Brown fat (g)	0.11 ± 0.01	0.10 ± 0.01
Blood glucose (mg/dL)	235.9 ± 11.7	148.4 ± 10.6*
Plasma insulin (ng/mL)	1.58 ± 0.23	1.32 ± 0.33
Liver triglyceride (μg/mg)	3.37 ± 0.15	3.74 ± 0.38
Plasma triglyceride (mg/dL)	155.9 ± 18.5	65.4 ± 3.9*
Plasma β-hydroxybutyrate (ng/mL)	3.42 ± 0.94	2.51 ± 0.19
Plasma free fatty acids (mEq/L)	0.79 ± 0.10	0.71 ± 0.05
Liver free fatty acids (mEq/mg protein)	0.096 ± 0.024	0.094 ± 0.030

3.3. Increased energy expenditure in *ACSL5*$^{-/-}$ mice

Both lines of mice consumed equivalent amounts of food (data not shown) indicating that food intake could not explain the differences in body composition. To determine if alterations in energy expenditure contributed to the differences in body composition we performed studies using indirect calorimetry. We observed that *ACSL5*$^{-/-}$ mice had significantly greater energy expenditure as compared to *ACSL5*$^{loxP/loxP}$ mice (Figure 4A). *ACSL5*$^{-/-}$ mice were also found to have a significantly higher respiratory exchange ratio (RER, Figure 4B) particularly during the early nighttime and early morning. An increase in RER is consistent with increased metabolism and utilization of carbohydrates. Despite the higher energy expenditure, male *ACSL5*$^{-/-}$ knockout mice and *ACSL5*$^{loxP/loxP}$ control mice were found to have equivalent activity levels (Figure 4C). In summary we observed that *ACSL5*$^{-/-}$ mice, as compared to *ACSL5*$^{loxP/loxP}$ mice, had increased energy expenditure; and by RER measurements these mice have increased utilization of glucose. Both parameters likely contribute to the improved metabolic profile of ACSL5 deficient mice.

3.4. *ACSL5*$^{-/-}$ mice have increased hepatic mRNA expression and serum levels of FGF21 and beige adipocyte formation

To determine a potential mechanistic basis for the phenotypic differences in the two lines of mice we analyzed the expression of several candidate genes. RT-PCR analysis of liver samples from *ACSL5*$^{-/-}$ mice revealed significant reductions in mRNA levels of two lipogenic genes, *Srebp1c* and *Scd1* as well as the nuclear transcription factor *Pparα* (Figure 5, top panel). Importantly, the level of fibroblast growth factor 21 (FGF21) mRNA was significantly increased in *ACSL5*$^{-/-}$ mice as compared to *ACSL5*$^{loxP/loxP}$ mice (Figure 5, top panel). FGF21 produced in the liver can be secreted resulting in increased circulating levels of FGF21 [22]. We found that circulating levels of FGF21 were potently increased in *ACSL5*$^{-/-}$ sera (7317 ± 842.5 ng/ml in *ACSL5*$^{-/-}$ vs. 550.8 ± 146.2 ng/ml in *ACSL5*$^{loxP/loxP}$), a more than 13-fold increase of FGF21 in *ACSL5*$^{-/-}$ mice (vs. *ACSL5*$^{loxP/loxP}$, $p < 0.0001$). As we noted in an earlier section, ablation of ACSL5 in liver resulted in increased *Acsl4* and reduced *Acsl1* mRNA expression (see Table 1), but the significance of these changes to the phenotype of the ACSL5 deficient mice is unclear.

Increased hepatic production and secretion of FGF21 has been linked to increased conversion of white adipocytes to beige adipocytes [22—24]. To confirm the conversion to beige adipocytes we performed RT-PCR analysis of gene expression in gonadal adipose tissue. Consistent with prior known actions of FGF21 we demonstrated increased mRNA levels of *Ucp1*, *Dio2*, *Pgc1α* and *Atgl* (Figure 5). FGF21 expression has also been reported to increase adiponectin expression, which, however, we did not observe [4,25]. In response to ACSL5 ablation in white adipose tissue, we observed increased levels of *Acsl1* mRNA (1.64 ± 0.28 fold increased ($p < 0.05$) in *ACSL5*$^{-/-}$ vs. *ACSL5*$^{loxP/loxP}$), which has been suggested to promote fat oxidation in adipocytes [5], as well as increased levels of *Acsl3* (2.03 ± 0.44 fold increased ($p < 0.05$) in *ACSL5*$^{-/-}$ vs. *ACSL5*$^{loxP/loxP}$). Our analysis of gene expression in brown adipose tissue demonstrated significantly increased *Dio2* mRNA levels in ACSL5 deficient mice, but no changes in *Ucp1*, *Ucp2*, and reduced *Pparα* transcript levels (Figure 5). As noted in Table 1, we noted no significant changes in any other ACSL isoforms in brown adipose tissue. In summary, both hepatic mRNA and circulating levels of FGF21 were significantly increased in ACSL5 deficient mice in association with increased white adipose tissue expression of UCP1 and oxidative genes.

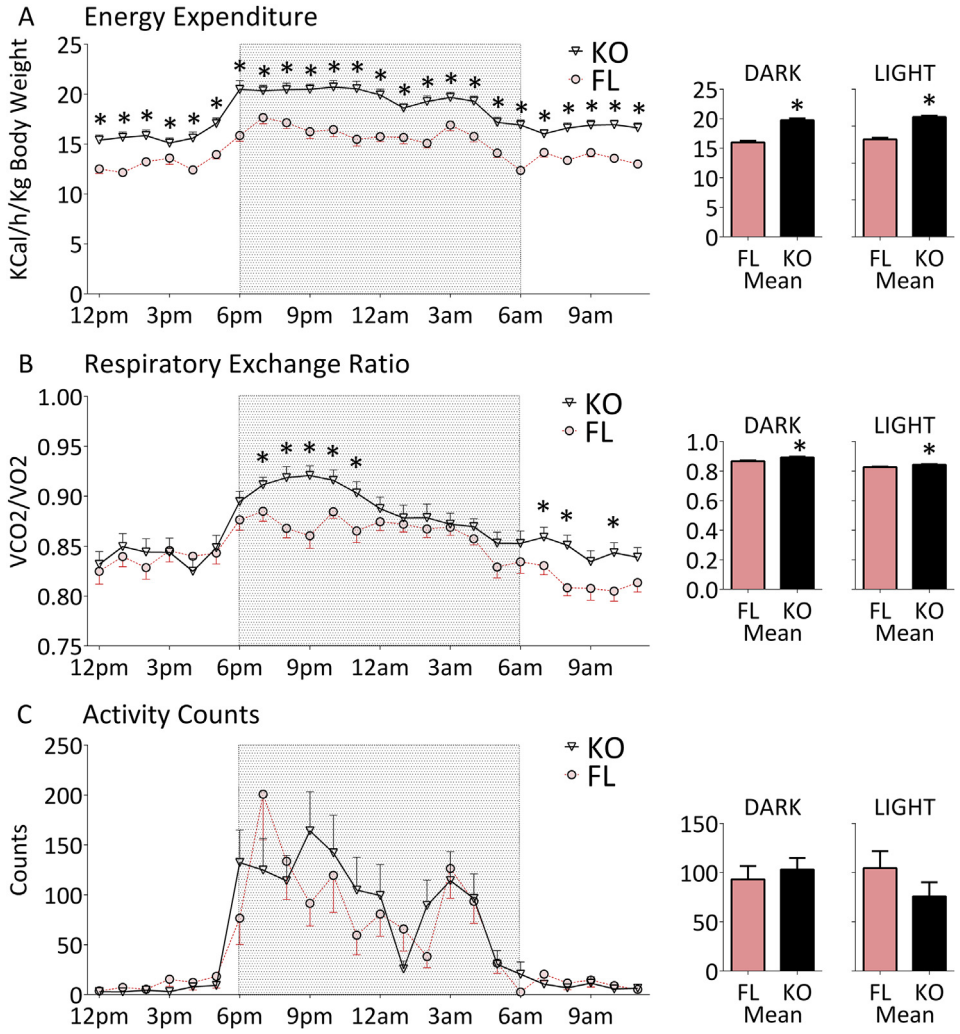

Figure 4: Increased energy expenditure of *ACSL5*$^{-/-}$ knockout mice. Mean ± SEM of energy expenditure (A), respiratory exchange ratio (B) and activity level (C) of four-month-old male mice were determined as in methods by indirect calorimetry in metabolic chambers (n = 8 mice per group average of 2 days after initial 24 h acclimation period). Dark and light phase cumulative means within dark or light phase and each time point were compared by student's t-test between *ACSL5*$^{-/-}$ (KO) and their littermate male *ACSL5*$^{loxP/loxP}$ floxed control (FL) mice, significance is indicated by *($p < 0.05$).

3.5. *ACSL5*$^{-/-}$ mice have altered kinetics of absorption of oral fat

ACSL5 is highly expressed in jejunum enterocytes [8], the cells critical for absorption and repackaging of fatty acids into triglycerides and chylomicrons for export ultimately to the circulation. We previously noted that ACSL5 ablation did not result in altered expression of other ACSL isoforms in the jejunal mucosa (see Table 1). Since we noted that ablation of ACSL5 reduced total ACSL activity in jejunal lysates by ~80% we investigated whether ACSL5 regulated the kinetics of fat absorption. For these studies, *ACSL5*$^{-/-}$ and *ACSL5*$^{loxP/loxP}$ mice were fasted for four hours, tyloxapol was injected to block peripheral lipoprotein lipase activity and then, mice were gavaged with an olive oil bolus. Blood was collected and the increase in serum triglyceride was then monitored over time [26]. We observed that in *ACSL5*$^{-/-}$ mice as compared to *ACSL5*$^{loxP/loxP}$ mice, the rate of increase in serum triglyceride after the oil bolus was reduced (Figure 6B). The altered absorption of serum triglyceride was not due to any differences in mRNA levels of *Fiaf*, *Scd1*, *Dgat1*, *Dgat2*, *Mgat*, or lipid droplet protein *Plin2* (Figure 6A). However, unexpectedly, we did note an increase in *Acot1* and *Hmgcs2* (by more than 7-fold) which are both regulated by activation of PPARα [27,28]. HMGCS2 regulates ketone body formation but we noted no increase in serum β-hydroxybutyrate (Table 1). Likely the lack of increase in serum ketones was because Hmgcs2 production in liver was not significantly different (Figure 5).

4. DISCUSSION

We now demonstrate in a newly generated line of ACSL5 deficient mice that the *in vivo* consequences of ACSL ablation are reduced adiposity, circulating triglyceride and glucose levels, as well as increased insulin sensitivity, energy expenditure, and reduced rate of intestinal triglyceride absorption. Remarkably, we observed potent increases in hepatic mRNA expression and circulating serum levels of FGF21, The increased circulating level of FGF21 was associated with the increased mRNA levels of *Ucp1*, consistent with effects of FGF21 to promote conversion of white to beige adipocytes, leading to increased rates of energy expenditure. The increased FGF21 levels may also explain the reduced serum blood glucose levels, since FGF21 has been noted to increase glucose uptake in brown adipose tissue [29].

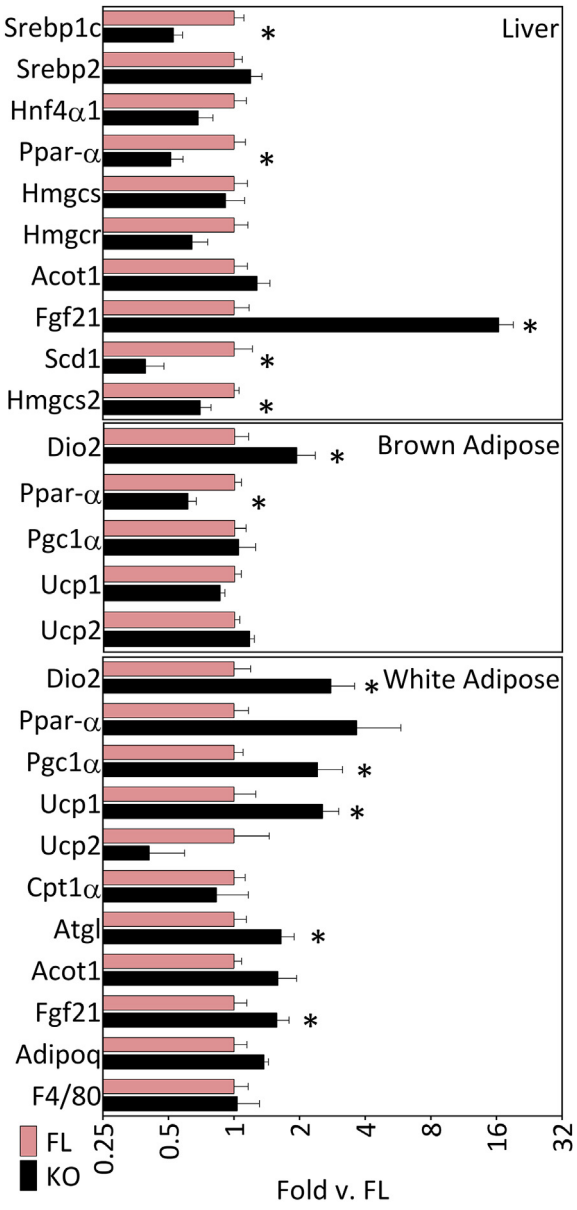

Figure 5: Gene expression profile *ACSL5*$^{-/-}$ knockout mice. Mean mRNA fold expression (see Methods) ± SEM of the liver, interscapular brown adipose tissue, and epididymal white adipose tissue of 5–7 mice were determined by semi-quantitative real-time RT-PCR, normalized to *Cyclophyllin B*, and normalized again to the mean result of each gene in floxed control *ASCL5*$^{loxP/loxP}$ (FL) mice samples; * ($p < 0.05$) indicates significant difference between $-\delta C_T$ values of ACSL5$^{loxP/loxP}$ and *ACSL5*$^{-/-}$ for each gene comparison.

Consistent with prior published studies, we also found that increased FGF21 levels resulted in reduced levels of serum triglycerides [29]. In addition to the phenotypic consequences of ACSL5 ablation we demonstrated significantly reduced total ACSL activity in liver, brown adipose tissue, and jejunum. ACSL5 is most highly expressed with intestinal mucosa and accounts for ~80% of total ACSL activity. To further investigate the role of ACSL5 in the intestine we performed an oral fat challenge study and noted that in ACSL5 deficient mice the rate of appearance of serum triglycerides was reduced as compared to control floxed mice. Our studies demonstrate that ACSL5 expression is an important regulator of metabolism and ACSL activity in several tissues and has significant effects on systemic metabolism.

Previous *in vitro* studies in hepatocytes have suggested that ACSL5 has a role in the accumulation and esterification of fatty acids into triglyceride. In one study using the McArdle cell line hepatocytes, ACSL5 was overexpressed incubated with exogenous fatty acids, fatty acid uptake as well as triglyceride accumulation were increased [7]. Of relevance, we observed that knockdown of ACSL5 expression in cultured rodent hepatocytes reduced rates of *de novo* lipogenesis, promoted fatty acid oxidation, and reduced triglyceride accumulation and secretion without evidence of PPARα activation [30]. In our present studies we fed mice a chow diet and noted no differences in serum or liver free fatty acids or liver triglyceride accumulation between the two lines of mice. Interestingly, in our studies on ACSL5 deficient mice, we observed that when ACSL5 expression is ablated in mice that both hepatic *Fgf21* mRNA expression and circulating levels of FGF21 were increased. In prior studies of the effects of ACSL5 knockdown in rodent hepatocytes, FGF21 expression was not investigated. Similar to studies investigating ACSL5 knockdown in isolated rat hepatocytes, we did not observe increased expression of hepatic genes downstream of the transcription factor, PPARα (for example, *Acot1* in Figure 5, top panel) [31], suggesting that the transcription factor, PPARα, was not activated. The initial studies identifying FGF21 demonstrated that it was a target of PPARα activation in liver [32,33]. At the present time the underlying mechanisms for the observed increase in FGF21 in ACSL5 deficient mice is not clear from the present studies. Future studies investigating the effects of tissue specific ablation of ACSL5 including hepatic ACSL5 ablation will focus on the causes for the increase in FGF21 levels.

In our present studies we noted that ACSL5 contributed significantly to the total ACSL activity in brown adipose tissue. Previous studies have demonstrated that ACSL5 is the predominant ACSL isoform in mitochondria of brown adipocytes [34] and that cold exposure significantly increased ACSL5 expression within mitochondria of brown adipocytes [34,35]. While ablation of ACSL5 reduced brown adipose total ACSL activity by approximately 37%, we noted an increase in *Dio2* mRNA but no increase in *Ucp1*, and a reduction in *Pparα* mRNA transcript levels. Since UCP1 expression was not changed in brown adipose tissue of ACSL5 deficient mice it is likely that the increased UCP1 in white adipocytes consistent with beiging of white adipose tissue contributes more to the observed increases in energy expenditure and reduced body fat content.

We observed that ACSL5 was most highly expressed in the jejunum [8] and that ablation of ACSL5 within jejunal mucosa reduced total ACSL activity by approximately 80%. Since ACSL activity is required in jejunum enterocytes for the reesterification of fatty acids into triglycerides, which are packaged and then exported as chylomicrons into the circulation, we challenged our lines of mice with an olive oil gavage and then measured serum triglycerides over time. In ACSL5 deficient mice we demonstrated that the rates of triglyceride appearance after the fat challenge were reduced. These studies suggest that ACSL5 expression within jejunal mucosa has a critical role in the absorption of fat. In future studies we will generate mice in which ACSL5 is specifically ablated within enterocytes to specifically determine the role of ACSL5 in the regulation of fatty acid absorption and the effect of intestinal ACSL5 ablation on systemic body composition and metabolism.

Previously another group generated mice in which exons 15–17 of ACSL5 were ablated to yield ACSL5 deficient mice [36]. However, while this group observed reductions in intestinal ACSL activity (60% vs. our 80% reduction), the researchers observed no alterations in rates of triglyceride appearance, body fat, and ACSL activity within the liver. It is quite possible that differing genetic backgrounds might

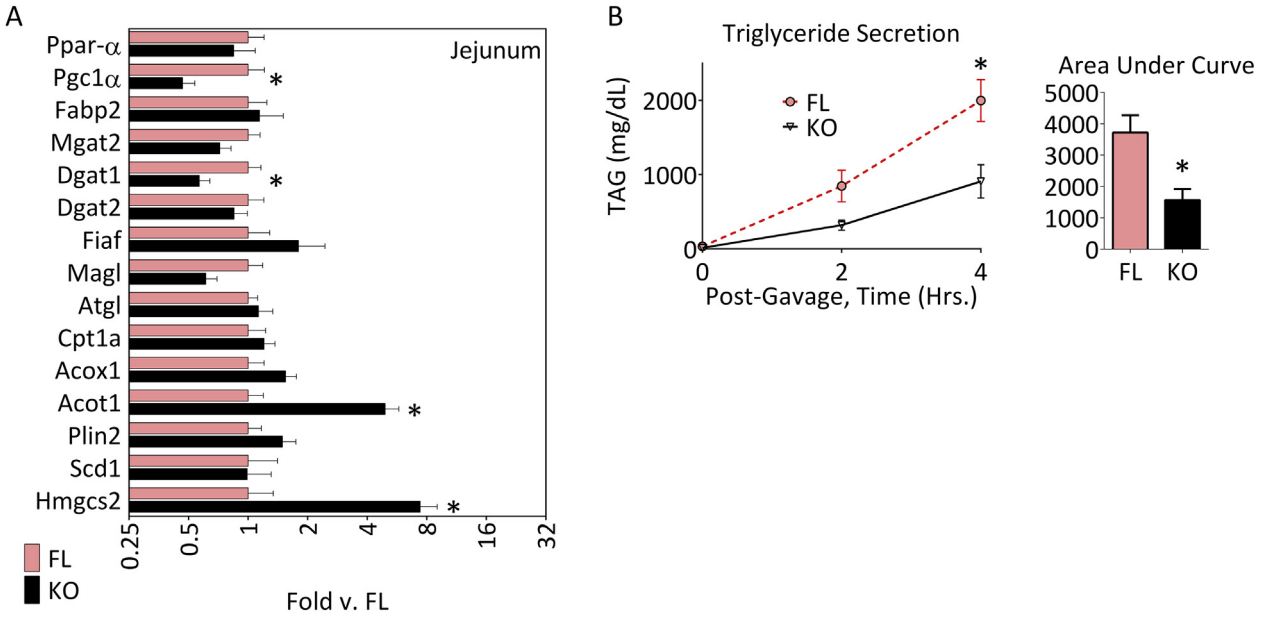

Figure 6: Intestinal gene expression profile and inhibition of triglyceride secretion in *ACSL5*$^{-/-}$ knockout mice. Mean mRNA fold expression (see Methods) ± SEM of mucosal scrapings of the second (middle third) section of the small intestine (A) of 5–7 mice after a 3 h morning fast were determined by semi-quantitative real-time RT-PCR, normalized to *Cyclophyllin B*, and normalized again to the mean result of each gene in floxed control *ASCL5*$^{loxP/loxP}$ (FL) mice samples; * ($p < 0.05$) indicates significant difference between $-\delta C_T$ values of *ACSL5*$^{loxP/loxP}$ and *ACSL5*$^{-/-}$ for each gene comparison. (B) Mean ± SEM plasma triglyceride concentrations and area under the curve for male, *ACSL5*$^{-/-}$ (KO) and littermate *ACSL5*$^{loxP/loxP}$ floxed control (FL) mice 2 and 4 h after an oral gavage of 200 μl of olive oil with inhibition of triglyceride clearance by tyloxapol (500 mg/kg); ($n = 4$ mice per group) *$p < 0.05$ for each time point and for area under the curve.

explain some of the observed phenotypic differences as our mice were on a pure C57BL6J background while the other mice were on a mixed C57BL6J/129sJ background. In our ACSL5 deficient mice we observed reduced total ACSL activity in liver extracts consistent with previous published studies showing that siRNA knockdown of ACSL5 in isolated hepatocytes significantly reduced total ACSL activity [12]. In the other paper describing ACSL5 deficient mice the authors did not report the expression of all of the other ACSL isoforms in their mouse livers, thus, another ACSL isoform may have compensated for any reductions in ACSL activity. Also, some of our studies differed in certain experimental approaches. For example, for our oral fat challenge we gavaged 200 μl of olive oil and measured triglyceride appearance over four hours. In contrast, in the prior publication, the group gavaged with 50 μl of olive oil and measured triglyceride appearance over only 90 min. We have observed that an oral gavage of 50 μl olive oil results in minimal triglyceride storage in lipid droplets in enterocytes [16]. Therefore if the function of ACSL5 relates to its localization on lipid droplets, a phenotype may not be observed in the deficiency of lipid droplets. Thus perhaps an olive oil bolus of 50 μl may not be of sufficient magnitude to delineate differences in rates of triglyceride appearance. The difference between a 50 μl and 200 μl olive oil bolus is similar to differences between a low fat or high fat diet typically fed to mice. It is possible that the role of ACSL5 in fat absorption varies between these two very different physiological conditions of a smaller olive oil bolus with shorter-term measurements or larger olive oil bolus with longer-term triglyceride serum measurements.

5. CONCLUSIONS

In summary, we now demonstrate that ablation of ACSL5 results in reduced adiposity, increased energy expenditure and circulating serum levels of FGF21, increased numbers of beige adipocytes and reduced rates of triglyceride absorption. Importantly, we demonstrate that ACSL5 contributes significantly to total ACSL activity within several tissues including brown adipose tissue, liver, and jejunal mucosa. Building upon these observations, future studies using tissue-specific knockout of ACSL5 are warranted to further define its local contribution to changes in energy metabolism.

ACKNOWLEDGMENTS

The authors wish to thank Rosalind M. Coleman and lab members, Trisha Grevengoed and Felecia S. Walton for their expert advice and training in assaying acyl CoA synthetase activity.

Funding: T.A.B. received support from the National Institute of Diabetes and Digestive and Kidney Diseases (NIDDK) (F32-DK-095538). T.D. receives support from the Purdue Research Foundation.

D.G.M. receives support from the NIDDK (DK-0903634) and the Minnesota Obesity Center (DK050456). K.K. B. receives support from the American Diabetes Association (7-13-IN-05), the Department of Defense, United States Army Medical Research Acquisition Activity (PC131237), and the Indiana Clinical and Translational Sciences Institute funded, in part by Grant Number Grant # UL1TR001108 from the National Institutes of Health, National Center for Advancing Translational Sciences, Clinical and Translational Sciences Award. A.S.G. receives support from NIEHS (UO1-ES-020958, RO3-ES-0227), NIDDK (R01 DK098606-02), NIDDK-Boston Nutrition Obesity Research Center (P30-DK-46200), T32 DK062032-24, and the U.S. Department of Agriculture, Agricultural Research Service, under agreement no. 58-1950-7-70. Dr. Greenberg is also the recipient of the Robert C and Veronica Atkins endowed Professorship in Nutrition and Metabolism at Tufts Medical School.

Duality of Interest: D.G.M. receives support from Novo Nordisk. No other potential conflicts of interest relevant to this article were reported.

CONFLICT OF INTEREST

None declared.

APPENDIX A. SUPPLEMENTARY DATA

Supplementary data related to this article can be found at http://dx.doi.org/10.1016/j.molmet.2016.01.001.

REFERENCES

[1] Greenberg, A.S., Coleman, R.A., Kraemer, F.B., McManaman, J.L., Obin, M.S., Puri, V., et al., 2011. The role of lipid droplets in metabolic disease in rodents and humans. Journal of Clinical Investigation 121(6):2102–2110.

[2] Savage, D.B., Petersen, K.F., Shulman, G.I., 2007. Disordered lipid metabolism and the pathogenesis of insulin resistance. Physiological Reviews 87(2):507–520.

[3] Glass, C.K., Olefsky, J.M., 2012. Inflammation and lipid signaling in the etiology of insulin resistance. Cell Metabolism 15(5):635–645.

[4] Ebbert, J.O., Jensen, M.D., 2013. Fat depots, free fatty acids, and dyslipidemia. Nutrients 5(2):498–508.

[5] Ellis, J.M., Frahm, J.L., Li, L.O., Coleman, R.A., 2010. Acyl-coenzyme A synthetases in metabolic control. Current Opinion in Lipidology 21(3):212–217.

[6] Mashek, D.G., Li, L.O., Coleman, R.A., 2007. Long-chain acyl-CoA synthetases and fatty acid channeling. Future Lipidology 2(4):465–476.

[7] Mashek, D.G., Li, L.O., Coleman, R.A., 2006. Rat long-chain acyl-CoA synthetase mRNA, protein, and activity vary in tissue distribution and in response to diet. Journal of Lipid Research 47(9):2004–2010.

[8] Oikawa, E., Iijima, H., Suzuki, T., Sasano, H., Sato, H., Kamataki, A., et al., 1998. A novel acyl-CoA synthetase, ACS5, expressed in intestinal epithelial cells and proliferating preadipocytes. Journal of Biochemistry 124(3):679–685.

[9] Achouri, Y., Hegarty, B.D., Allanic, D., Becard, D., Hainault, I., Ferre, P., et al., 2005. Long chain fatty acyl-CoA synthetase 5 expression is induced by insulin and glucose: involvement of sterol regulatory element-binding protein-1c. Biochimie 87(12):1149–1155.

[10] Haas, J.T., Miao, J., Chanda, D., Wang, Y., Zhao, E., Haas, M.E., et al., 2012. Hepatic insulin signaling is required for obesity-dependent expression of SREBP-1c mRNA but not for feeding-dependent expression. Cell Metabolism 15(6):873–884.

[11] Horton, J.D., Goldstein, J.L., Brown, M.S., 2002. SREBPs: activators of the complete program of cholesterol and fatty acid synthesis in the liver. Journal of Clinical Investigation 109(9):1125–1131.

[12] Bu, S.Y., Mashek, D.G., 2010. Hepatic long-chain acyl-CoA synthetase 5 mediates fatty acid channeling between anabolic and catabolic pathways. Journal of Lipid Research 51(11):3270–3280.

[13] D'Aquila, T., Sirohi, D., Grabowski, J.M., Hedrick, V.E., Paul, L.N., Greenberg, A.S., et al., 2015. Characterization of the proteome of cytoplasmic lipid droplets in mouse enterocytes after a dietary fat challenge. PLoS One 10(5):e0126823.

[14] Lee, B., Fast, A.M., Zhu, J., Cheng, J.X., Buhman, K.K., 2010. Intestine-specific expression of acyl CoA:diacylglycerol acyltransferase 1 reverses resistance to diet-induced hepatic steatosis and obesity in Dgat1-/- mice. Journal of Lipid Research 51(7):1770–1780.

[15] Uchida, A., Lee, H.J., Cheng, J.X., Buhman, K.K., 2013. Imaging cytoplasmic lipid droplets in enterocytes and assessing dietary fat absorption. Methods in Cell Biology 116:151–166.

[16] Zhu, J., Lee, B., Buhman, K.K., Cheng, J.X., 2009. A dynamic, cytoplasmic triacylglycerol pool in enterocytes revealed by ex vivo and in vivo coherent anti-Stokes Raman scattering imaging. Journal of Lipid Research 50(6):1080–1089.

[17] Grevengoed, T.J., Cooper, D.E., Young, P.A., Ellis, J.M., Coleman, R.A., 2015 Nov. Loss of long-chain acyl-CoA synthetase isoform 1 impairs cardiac autophagy and mitochondrial structure through mechanistic target of rapamycin complex 1 activation. FASEB Journal 29(11):4641–4653. http://dx.doi.org/10.1096/fj.15-272732. [Epub 2015 Jul 28].

[18] Kim, J.H., Lewin, T.M., Coleman, R.A., 2001. Expression and characterization of recombinant rat Acyl-CoA synthetases 1, 4, and 5. Selective inhibition by triacsin C and thiazolidinediones. The Journal of Biological Chemistry 276(27):24667–24673.

[19] Folch, J., Lees, M., Sloane Stanley, G.H., 1957. A simple method for the isolation and purification of total lipides from animal tissues. The Journal of Biological Chemistry 226(1):497–509.

[20] Frayn, K.N., Maycock, P.F., 1980. Skeletal muscle triacylglycerol in the rat: methods for sampling and measurement, and studies of biological variability. Journal of Lipid Research 21(1):139–144.

[21] Spriet, L.L., Heigenhauser, G.J., Jones, N.L., 1986. Endogenous triacylglycerol utilization by rat skeletal muscle during tetanic stimulation. Journal of Applied Physiology (1985) 60(2):410–415.

[22] Markan, K.R., Naber, M.C., Ameka, M.K., Anderegg, M.D., Mangelsdorf, D.J., Kliewer, S.A., et al., 2014. Circulating FGF21 is liver derived and enhances glucose uptake during refeeding and overfeeding. Diabetes 63(12):4057–4063.

[23] Owen, B.M., Ding, X., Morgan, D.A., Coate, K.C., Bookout, A.L., Rahmouni, K., et al., 2014. FGF21 acts centrally to induce sympathetic nerve activity, energy expenditure, and weight loss. Cell Metabolism 20(4):670–677.

[24] Fisher, F.M., Kleiner, S., Douris, N., Fox, E.C., Mepani, R.J., Verdeguer, F., et al., 2012. FGF21 regulates PGC-1alpha and browning of white adipose tissues in adaptive thermogenesis. Genes & Development 26(3):271–281.

[25] Holland, W.L., Adams, A.C., Brozinick, J.T., Bui, H.H., Miyauchi, Y., Kusminski, C.M., et al., 2013. An FGF21-adiponectin-ceramide axis controls energy expenditure and insulin action in mice. Cell Metabolism 17(5):790–797.

[26] Uchida, A., Whitsitt, M.C., Eustaquio, T., Slipchenko, M.N., Leary, J.F., Cheng, J.X., et al., 2012. Reduced triglyceride secretion in response to an acute dietary fat challenge in obese compared to lean mice. Frontiers in Physiology 3:26.

[27] Uchida, A., Slipchenko, M.N., Cheng, J.X., Buhman, K.K., 2011. Fenofibrate, a peroxisome proliferator-activated receptor alpha agonist, alters triglyceride metabolism in enterocytes of mice. Biochimica et Biophysica Acta 1811(3):170–176.

[28] Bunger, M., van den Bosch, H.M., van der Meijde, J., Kersten, S., Hooiveld, G.J., Muller, M., 2007. Genome-wide analysis of PPARalpha activation in murine small intestine. Physiological Genomics 30(2):192–204.

[29] Emanuelli, B., Vienberg, S.G., Smyth, G., Cheng, C., Stanford, K.I., Arumugam, M., et al., 2014. Interplay between FGF21 and insulin action in the liver regulates metabolism. Journal of Clinical Investigation 124(2):515–527.

[30] Bu, S.Y., Mashek, M.T., Mashek, D.G., 2009. Suppression of long chain acyl-CoA synthetase 3 decreases hepatic de novo fatty acid synthesis through decreased transcriptional activity. The Journal of Biological Chemistry 284(44):30474–30483.

[31] Rakhshandehroo, M., Hooiveld, G., Muller, M., Kersten, S., 2009. Comparative analysis of gene regulation by the transcription factor PPARalpha between mouse and human. PLoS One 4(8):e6796.

[32] Badman, M.K., Pissios, P., Kennedy, A.R., Koukos, G., Flier, J.S., Maratos-Flier, E., 2007. Hepatic fibroblast growth factor 21 is regulated by PPARalpha and is a key mediator of hepatic lipid metabolism in ketotic states. Cell Metabolism 5(6):426–437.

[33] Inagaki, T., Dutchak, P., Zhao, G., Ding, X., Gautron, L., Parameswara, V., et al., 2007. Endocrine regulation of the fasting response by PPARalpha-

mediated induction of fibroblast growth factor 21. Cell Metabolism 5(6): 415–425.

[34] Forner, F., Kumar, C., Luber, C.A., Fromme, T., Klingenspor, M., Mann, M., 2009. Proteome differences between brown and white fat mitochondria reveal specialized metabolic functions. Cell Metabolism 10(4):324–335.

[35] Yu, X.X., Lewin, D.A., Forrest, W., Adams, S.H., 2002. Cold elicits the simultaneous induction of fatty acid synthesis and {beta}-oxidation in murine brown adipose tissue: prediction from differential gene expression and confirmation in vivo. FASEB Journal 16(2):155–168.

[36] Meller, N., Morgan, M.E., Wong, W.P., Altemus, J.B., Sehayek, E., 2013. Targeting of Acyl-CoA synthetase 5 decreases jejunal fatty acid activation with no effect on dietary long-chain fatty acid absorption. Lipids in Health and Disease 12:88.

